https://doi.org/10.5194/amt-2021-436
Preprint. Discussion started: 14 January 2022

Atmospheric Measurement Techniques Discussions
Open Access
EGU

Characterization of tandem aerosol classifiers for selecting particles: implication for eliminating multiple charging effect

Yao Song[1], Xiangyu Pei[1], Huichao Liu[1], Jiajia Zhou[1], Zhibin Wang[1,2,3,4*]

[1]College of Environmental and Resource Sciences, Zhejiang University, Hangzhou, 310058, China
[2]Hangzhou Global Scientific and Technological Innovation Center, Zhejiang University, Hangzhou, 311200, China
[3]Zhejiang Provincial Key Laboratory of Organic Pollution Process and Control, Hangzhou 310058, China.
[4]Key Laboratory of Environment Remediation and Ecological Health, Ministry of Education, Zhejiang University, 310058 Hangzhou, China

correspondence to: Zhibin Wang (wangzhibin@zju.edu.cn)

Abstract. Accurate particle classification plays a vital role in aerosol studies. Differential mobility analyzer (DMA), centrifugal particle mass analyzer (CPMA) and aerodynamic aerosol classifier (AAC) are commonly used to select particles with a specific size or mass. However, multiple charging effect cannot be entirely avoided either using individual technique or using tandem system such as DMA-CPMA, especially when selecting soot particles with fractal structures. In this study, we demonstrate the transfer functions of DMA-CPMA and DMA-AAC systems, as well as the potential multiple charging effect. Our results show that the ability to remove multiply charged particles mainly depends on particles morphology and instruments setups of DMA-CPMA system. Using measurements from soot experiments and literature data, a general trend in the appearance of multiple charging effect with decreasing size when selecting aspherical particles was observed. Otherwise, our results indicated that the ability of DMA-AAC to resolve particles with multiple charges is mainly related to the resolutions of classifiers. In most cases, DMA-AAC can eliminate multiple charging effect regardless of the particle morphology, while particles with multiple charges can be selected when decreasing resolutions of DMA and AAC. We propose that the multiple charging effect should be reconsidered when using DMA-CPMA or DMA-AAC system in estimating size and mass resolved optical properties in the field and lab experiments.

1 Introduction

Atmospheric aerosol particles span a wide size range from 1 nm to > 100 µm. Significant size dependence of aerosol physicochemical properties has been widely reported. Particle size can strongly alters the hygroscopic behavior (Biskos et al., 2006), phase state (Cheng et al., 2015) and cloud-nucleating ability (Dusek et al., 2006) of aerosol nanoparticles, indicating its importance when assessing the climate effect. Hence, accurate particle classification is essential to investigate the size dependence behavior of aerosol particles.

https://doi.org/10.5194/amt-2021-436
Preprint. Discussion started: 14 January 2022

At present, particles are generally classified by either size or mass in atmospheric aerosol studies. Differential mobility analyzer (DMA) is the most commonly used size classifier, which selects particles based on the electrical mobility (Knutson and Whitby, 1975). Particle mass analyzer (PMA) includes the aerosol particle mass analyzer (APM) and the centrifugal particle mass analyzer (CPMA), both of which classify particles based on their mass-to-charge ratio (Ehara et al., 1996; Olfert and Collings, 2005). However, particles are required to be pre-charged when classified by the DMA or PMA, resulting in that particles with higher-order charges and identical apparent mobility or mass-to-charge ratio will be selected simultaneously, which are referred to as the multiple charging effect. This may introduce uncertainty in the subsequence characterization. Radney et al. (2013) demonstrated that although the single-charged particles account for the highest number fraction (46.3%) of the DMA-classified particles (200 nm), while their contributions to the total mass concentration and extinction are insignificant (10.8% and 7.96%, respectively). Thus, the reported extinction of particles with a certain diameter was greatly overestimated due to the multiple charging effect.

Previous studies (Shiraiwa et al., 2010;Rissler et al., 2013; Johnson et al., 2014; Johnson et al., 2021) tried to utilize the combination of size and mass classifiers, like DMA-APM or DMA-CPMA system, to obtain singly charged particles. Theoretically, the ability of DMA-APM to eliminate multiply charged particles is governed by the particles morphology and setups of DMA-APM (Kuwata, 2015). This conclusion implies that it can hardly to achieved that all the multiply charged particles are effectively excluded for aspherical particles, especially for soot particles. Radney and Zangmeister (2016) conducted the limitation of DMA-APM with three types of particles (polystyrene Latex spheres (PSL), ammonia sulfate (AS) and soot particles), the results demonstrated that DMA-APM can resolve multiply charged particles for spherical particles (PSL and AS particles), but it failed for aspherical soot particles. Multiply charged soot particles led to over 110% errors in retrieving mass specific extinction cross section.

In contrast to DMA and PMA, aerodynamic aerosol classifier (AAC) is a novel instrument which selects aerodynamic equivalent diameter of aerosol particles based on their relaxation time. The advantage of utilizing AAC is that no charging process is needed in particle classification compared with the aforementioned classifiers, hence the multiple charging effects can be avoided (Tavakoli and Olfert, 2013). Morphology information, such as effective density (ρ_{eff}), mass-mobility exponent(D_{fm}) and dynamic shape factor (χ), can be inferred using the tandem systems of DMA-PMA (Park et al., 2003;Zhang et al., 2008;Rissler et al., 2013;Pei et al., 2018;Zangmeister et al., 2018), DMA-AAC (Tavakoli and Olfert, 2014) and AAC-CPMA (Johnson et al., 2018), respectively.

The theoretical transfer functions of individual classifier (DMA, CPMA and AAC) and DMA-APM system have been previously discussed (Knutson and Whitby, 1975; Ehara et al., 1996; Olfert and Collings, 2005; Stolzenburg and McMurry, 2008; Tavakoli and Olfert, 2013). In this study, we calculated the transfer functions of DMA-AAC and DMA-CPMA systematically. Combined with soot experiments, we demonstrated that multiple charging effects may still exist after DMA-CPMA classification when selecting aspherical particles, and evaluated the light absorption of selected particles with different charging states using Mie theory. Furthermore, we proposed the operating condition for DMA-CPMA to eliminate the

https://doi.org/10.5194/amt-2021-436
Preprint. Discussion started: 14 January 2022

Atmospheric Measurement Techniques Discussions

multiply charged particles in the future studies. Our results suggest that the size- and mass-resolved optical properties may be overestimated for small soot particles when using DMA-CPMA system, which will lower the accuracy of predicting soot climate effect.

2 Theory and experiment

2.1 Transfer function for individual aerosol classifier

DMA

The DMA, consisting of two coaxial electrodes, classifies particle based upon electrical mobility Z_p (Knutson and Whitby, 1975), which can be calculated as follows:

$$Z_p = q\mathrm{B} = \frac{neCc(d_p)}{3\pi\mu d_p}, \quad (1)$$

where q is the particle charge, n is the number of particle charges, B is the mobility of particle, e is the elemental charge, μ is the viscosity of the air, $Cc(d_p)$ is the Cunningham slip correction factor. When aerosol inlet flow rate equals to aerosol sampling outlet flow rate, the Z_p* selected by the DMA is defined as

$$Z_p^* = \frac{Q_{sh}}{2\pi V_{DMA} L_{DMA}} \ln\left(\frac{r_{2\_DMA}}{r_{1\_DMA}}\right), \quad (2)$$

where Q_{sh} is the sheath flow rate, V_{DMA} is the voltage between the two electrodes, L_{DMA} is the length of DMA, r_{1_DMA} and r_{2_DMA} are the inner and outer radii of DMA, respectively. The transfer function of DMA can be expressed as follows when particle diffusion is negligible (Knutson and Whitby, 1975; Stolzenburg and McMurry, 2008),

$$\Omega\left(\widetilde{Z_p}, \beta_{DMA}\right) = \frac{1}{2\beta_{DMA}}\left[\left|\widetilde{Z_p} - (1+\beta_{DMA})\right| + \left|\widetilde{Z_p} - (1-\beta_{DMA})\right| - 2\left|\widetilde{Z_p} - 1\right|\right], \quad (3)$$

where the $\widetilde{Zp} = Z_p/Z_p^*$, $\beta_{DMA}=Q_a/Q_{sh}$, and Q_a is the sample flow rate. The transfer function is an isosceles triangle with value of 1 at Z_p^* and going to 0 at $(1 \pm \beta_{DMA})\cdot Z_p^*$.

CPMA

The construction of CPMA is similar to the APM, but its inner cylinder rotates faster than outer one to create a stable system of forces (Olfert and Collings, 2005). In the CPMA, the equation of particles motion is expressed as

$$\frac{m}{\tau}\frac{dr}{dt} = \frac{mv_\theta(r)^2}{r} - \frac{qV_{CPMA}}{r\ln\left(\frac{r_{2\_CPMA}}{r_{1\_CPMA}}\right)}, \quad (4)$$

and the trajectory equation is

$$\frac{dr}{dz} = \frac{dr}{dt}\left(\frac{dz}{dt}\right)^{-1} = \frac{c_r}{v_z}, \quad (5)$$

where τ is the relaxation time, m is the mass of the particle, t is time, V is the voltage difference between the two electrodes, r_{1_CPMA} and r_{2_CPMA} are the radii of inner and outer electrodes, respectively. c_r is particle migration velocity, v_z is the axial flow distribution and v_θ is the velocity profile in the angular direction,

$$v_\theta = \omega_1 \frac{\hat{r}^2 - \hat{\omega}}{\hat{r}^2 - 1} r + \omega_1 r_{1\_CPMA}^2 \frac{\hat{\omega} - 1}{\hat{r}^2 - 1}\frac{1}{r} = \alpha r + \frac{\beta}{r}, \quad (6)$$

https://doi.org/10.5194/amt-2021-436
Preprint. Discussion started: 14 January 2022

where $\hat{\omega} = \omega_2/\omega_1$ is the ratio of the rotational speed of the outer electrode to the inner electrode and ω_1 and ω_2 are the rotational speed of the inner and outer electrode, respectively. $\hat{r}$ is the ratio of the inner and outer radius.

Sipkens et al. (2019) gave the methods to calculate the transfer function of CPMA. They proposed that the Taylor series expansion at the center of the gap ($r_c=(r_{2\_CPMA}+r_{1\_CPMA})/2$) is much simpler and more robust. In this case, the particle migration velocity in the radical direction is

$$c_r \approx C_3 + C_4(r - r_c)\ , \tag{7}$$

where

$$C_3 = \tau\left(\alpha^2 r_c + \frac{2\alpha\beta}{r_c} + \frac{\beta^2}{r_c^3} - \frac{C_0}{m r_c}\right), \tag{8}$$

$$C_4 = \tau\left(\alpha^2 - \frac{2\alpha\beta}{r_c} - \frac{3\beta^2}{r_c^4} + \frac{C_0}{m r_c^2}\right), \tag{9}$$

$$C_0 = \frac{qV_{CPMA}}{\ln(r_{2\_CPMA}/r_{1\_CPMA})}, \tag{10}$$

Assuming a plug flow, the transfer function should be

$$\Omega = \frac{r_b - r_a}{2\delta}, \tag{11}$$

where $\delta=(r_{2\_CPMA}-r_{1\_CPMA})/2$ is the half width of the gap between the two electrodes, and

$$r_a = \min\left\{r_{2\_CPMA}, max\{r_{1\_CPMA}, G_0(r_{1\_CPMA})\}\right\}, \tag{12}$$

$$r_b = \min\left\{r_{2\_CPMA}, max\{r_{1\_CPMA}, G_0(r_{2\_CPMA})\}\right\}, \tag{13}$$

$$G_0(r_L) = r_c + \left(r_L - r_c + \frac{C_3}{C_4}\right)\exp(-C_4 L\bar{v}) - \frac{C_3}{C_4}, \tag{14}$$

where $G_0(r)$ is the operator to map the final radial position of the particle to its position at the inlet, $\bar{v}$ is average flow velocity.

Reavell et al. (2011) calculated the resolution of CPMA assuming that the gap between two electrodes is narrow enough that variation of force in the gap can be ignored. The limiting mass can be calculated by

$$m_{1,min}^{1,max}\omega^2 r - qE = \pm\frac{Q_{CPMA}}{2\pi B_{1,min}^{1,max} L_{CPMA} r_c^2 \omega^2}, \tag{15}$$

where ω is the equivalent rotational speed calculated by $\omega = \alpha + \frac{\beta}{r_c^2}$, $m_{1,min}^{1,max}$ and $B_{1,min}^{1,max}$ are the maximum and minimum mass and corresponding mobility with single charge that CPMA can select, respectively. Further details can be found in Reavell et al. (2011) and Sipkens et al. (2019).

AAC

The AAC classifies particle based on relaxation time, which is defined by

$$\tau = Bm = \frac{Cc(d_{ae})\rho_0 d_{ae}^2}{18\mu}, \tag{16}$$

where μ is the viscosity of air. $Cc(d_{ae})$ is the slip correction factor. ρ_0 is the standard density with value of 1 g/cm^3 (Johnson et al. 2018). When aerosol inlet flow rate equals to aerosol sampling outlet flow rate, it can be expressed as (Tavakoli and Olfert, 2013)

$$\Omega = \frac{1}{2\beta_{AAC}}\left[|\tilde{\tau} - (1 - \beta_{AAC})| + |\tilde{\tau} - (1 + \beta_{AAC})| - 2|\tilde{\tau} - 1|\right], \tag{17}$$

https://doi.org/10.5194/amt-2021-436
Preprint. Discussion started: 14 January 2022

τ^* is the nominated relaxation time which is classified by the AAC,

$$\tau^* = \frac{2Q_{sh}}{\pi\omega^2(r_{1\_AAC}+r_{\_2AAC})^2 L}, \quad (18)$$

where $\beta_{AAC} = \frac{Q_a}{Q_{sh}}$, $\tilde{\tau} = \frac{\tau}{\tau^*}$, r_{1_AAC} and r_{2_AAC} are the inner and outer radii of AAC, respectively.

2.2 Experimental setup

A schematic of the experimental setup is illustrated in Fig. 1. Soot particles were generated by a miniature inverted soot generator (Argonaut Scientific Ltd., Canada). Detailed aerosol generation methods can be found in Moallemi et al. (2019). The poly-dispersed aerosols were dried to a relative humidity of <20% by a silica dryer, and then were passed through a soft X-ray neutralizer (Model 3088, TSI, Inc., USA). Five mobility diameters (80, 100, 150, 200 and 250 nm) of soot particles were selected with DMA (Model 3081, TSI Inc., USA, $Q_{sh}/Q_a = 10$). For the soot characterization, the monodisperse aerosol flow was switched between two parallel lines and fed into CPMA (Cambustion Ltd., UK) and AAC (Cambustion, Ltd., UK, $Q_{sh}/Q_a = 10$), respectively. The particles mass (m) and aerodynamic diameter (d_{ae}) were determined by stepping mode of CPMA and AAC while the condensation particle counter (CPC, Model 3756, TSI, Inc., USA) recorded their corresponding concentration at each setpoint, respectively. The m and d_{ae} distributions were measured and fitted to log-normal distribution, thus the mode m and d_{ae} for the mobility-selected particles were determined. CPMA and AAC were calibrated with certified PSL spheres (Thermo, USA) with sizes of 70, 150 and 303 nm before the measurement. The measured m and d_{ae} were compared to m_{PSL} and $d_{ae,\ PSL}$ which were calculated with the nominal diameter and density of PSL. The deviations between measured m and m_{PSL} or measured d_{ae} and $d_{ae,\ PSL}$ were 2.75% and 5.14%, respectively. In order to quantify the multiple charging effect of particles selected by DMA-CPMA system, the d_{ae} distribution of twice classified particles was obtained by stepping the AAC rotation speed of the cylinder with simultaneous measurement of the particle concentration at the AAC outlet using a CPC (Fig. 1b).

3 Results and discussion

3.1 Transfer function of the tandem system

The DMA, PMA and AAC select particles based on the electrical diameter, mass and aerodynamic diameter, respectively. These properties can be connected as follows (Decarlo et al. 2004)

$$\frac{Cc(d_{ae})\rho_0 d_{ae}^2}{6} = \frac{Cc(d_m)\rho_{eff} d_m^2}{6} = m\frac{Cc(d_m)}{\pi d_m}, \quad (19)$$

The transfer function of DMA-APM has been well documented, which can be found in Kuwata (2015). The convolution of transfer functions of DMA-CPMA and DMA-AAC were calculated by the following equations.

$$\Phi_{\mathrm{DMA-CPMA}} = \Omega_{CPMA}\Omega_{DMA}, \quad (20)$$

$$\Phi_{\mathrm{DMA-AAC}} = \Omega_{DMA}\Omega_{AAC}, \quad (21)$$

https://doi.org/10.5194/amt-2021-436
Preprint. Discussion started: 14 January 2022

Atmospheric Measurement Techniques Discussions

where Φ and Ω are the transfer functions of each classification system expressed by subscript. In the following discussion, we explain the transfer functions of DMA-CPMA and DMA-AAC utilizing the literature data of soot particles (Pei et al., 2018). The d_m and m of the representative particles are 100 nm and 0.33 fg, respectively, and the corresponding d_{ae} is 68.3 nm according to Eq. (19). The dimension of individual classifier is summarized in Table 1.

DMA-CPMA

DMA-CPMA transfer function was calculated in the log(d_m)-log(m) space, as shown in Fig. 2. In the log(d_m)-log(m) space, the mass-mobility relationship is

$$m = \rho_f {d_m}^{D_{fm}} , \quad (22)$$

$$\log(m) = D_{\text{fm}} \log(d_m) + \log(\rho_f) , \quad (23)$$

In theory, D_{fm} equals to 3 for spherical particles and smaller than 3 for aspherical particles. In the log(d_m)-log(m) space, the relationship of m and d_m is linear with the slope expressed as mass-mobility exponent (D_{fm}) and the intercept representing pre-exponential factor (ρ_f). Under this specific operation condition, no overlap was observed between spherical particles population (black line) and the classification region for doubly charged particles, implying only the singly charged particles were selected. However, for aspherical particles with $D_{fm} < 3$, such as soot particles with aggregate structure, the particles population may overlap the doubly charged region when the slope (D_{fm}) is small enough, however, the combination of DMA and CPMA is generally used to avoid the multiple charge effect in soot studies. The reported D_{fm} values are typically in the range of 2.2-2.4 for fresh soot particles (Rissler et al., 2013) and diesel soot particles (Park et al., 2003). In the exemplary case, the derived D_{fm} of premixed flame generated soot particles was 2.28, resulting in the particles population always goes through the transfer area of doubly charged particles. This implies that the performance of DMA-CPMA to eliminate multiple-charged particles to a certain extent depends on the particle morphology.

The DMA-CPMA system can eliminate the multiply charged particles only if the D_{fm} of particles is larger than the slope of a line connecting (d_m, m) = ($d_{m2,\min}$, $m_{2,\max}$)(d_{m1},m_1) (as PP_0 shown in Fig. 2). Since CPMA is used downstream of the DMA, the value of mass limit can be expressed as follows according to Eq. (15) assuming that all the classified particles have the same mobility.

$$m_{n,min}^{n,max} = n \cdot m_1 \pm \frac{Q_{\text{CPMA}}}{2\pi B_{n,min}^{n,max} L_{\text{CPMA}} r_c^2 \omega^2} , \quad (24)$$

where $m_{n,min}^{n,max}$ and $B_{n,min}^{n,max}$ are the maximum and minimum particle mass and mechanical mobility which would be selected by CPMA and DMA, respectively. The subscript n is charge quantity. Accordingly, the ideal condition to completely eliminate the multiply charged particles is

$$D_{fm} > PP_0 = \frac{\log(m_{2,max}/m_1)}{\log(d_{m2,min}/d_{m1})} = \frac{log\left(2 + \frac{3Q_{CPMA}\mu d_{m1}}{(1-\beta_{DMA})L_{CPMA} r_c^2 \omega^2 m_1 Cc(d_{m1})}\right)}{log\left(\frac{2}{(1-\beta_{DMA})} \frac{Cc(d_{m2,min})}{Cc(d_{m1})}\right)} , \quad (25)$$

The ability of DMA-CPMA to eliminate multiply charged particles depends on the selected d_m, m and resolutions of both DMA and CPMA. The Eq. (25) gives instructions in actual operation to eliminate multiple-charged particles. When selecting particles of certain d_m and m, the smaller Q_{CPMA}, as well as larger

https://doi.org/10.5194/amt-2021-436
Preprint. Discussion started: 14 January 2022

ω and β_{DMA} are necessary to reduce the potential of multiply charged particles. Thus, the key to evaluate whether there is multiple charging effect lies on particle morphology (D_{fm}) and the slope of PP_0 derived from the actual condition. Compared with DMA-CPMA, the selection of DMA-APM is more susceptible to multiple charging effect. According to the theoretical calculation described in Kuwata (2015), the slope of PP_0 of 3.55 was derived when DMA-APM selects the same example soot particles (d_m of 100 nm and m of 0.33 fg) with D_{fm} of 2.28, indicating that the DMA-APM is more subjected to the multiple charging effect.

Besides the instruments setups, particles morphology is also crucial for DMA-CPMA. Here we simulate the critical slope of PP_0 when selecting different d_m and m under the common selecting conditions (β_{DMA} = 0.1, Q_{CPMA}=0.3 L min^{-1}, R_m = 8), which is shown in Fig. 3. Under this selecting conditions, DMA-CPMA can select monodispersed particles when the D_{fm} of particles is larger than the slope of PP_0 which is represented as background color. When selecting small aspherical particles or particles with extremely low density, the slope of PP_0 is relatively higher and DMA-CPMA classification is sensitive to multiple charging effect. As shown in Fig. 3, the d_m, m and corresponding D_{fm} were taken from literature (Park et al., 2003; Rissler et al., 2013; Ait Ali Yahia et al., 2017; Dastanpour et al., 2017; Kazemimanesh et al., 2019). Generally, multiple charging effect can be avoided for DMA-CPMA to select soot particles with diameter larger than 200 nm., while fails to eliminate multiply charged particles when selecting small soot particles. The potential uncertainties will be discussed in details with flame generated soot particles in Sect. 3.2.

DMA-AAC

The advantage of AAC versus CPMA is there is no need for a neutralizer to charge aerosol particles. Therefore, the multiple charge effect could be avoided theoretically. The transfer function of DMA-AAC selecting the same representing particles was calculated and shown in log(d_{ae})-log(d_m) (Fig. 4a). Moreover, according to Eqn. 19 and Eqn. 22, aspherical particles can be expressed as follows,

$$log d_{ae} = \frac{1}{2}\left(D_{fm} - 1\right) log d_m + \frac{1}{2}\log\left(\frac{6}{\pi}\frac{Cc(d_m)\rho_f}{Cc(d_{ae})\rho_0} \cdot 10^{9D_{fm}-18}\right), \quad (26)$$

which indicates that the relationship between d_{ae} and d_m is non-linear since the $Cc(d_m)$ and $Cc(d_{ae})$ varies with d_m and d_{ae}, respectively. Particles morphology can be derived from the relationship between d_m and d_{ae} measured by DMA and AAC, respectively. In order to simulate the transfer function of DMA-AAC selecting the same particles as that used in calculations of DMA-CPMA. The corresponding d_{ae} was numerically solved using known mass-size relationship. Unlike the DMA-CPMA system, the transfer functions of singly charged and doubly charged particles is in parallel for DMA-AAC, suggesting that particle population is less likely to overlap with the region of multiply charged particles. Using the example setups of DMA-AAC, truly monodispersed particles are selected for spherical particles and typical soot particles.

Similar to the DMA-CPMA system, to eliminate multiply charged particles requires the $d_{ae,max}$ of the AAC at $d_{m2,min}$ must be smaller than the d_{ae} of particles of interest which can be derived from $d_{m2,min}$ and D_{fm} (Eqn. 26),

$$d_{ae}\left(d_{m2,min}, D_{fm}\right) > d_{ae,max}\left(d_{m2,min}\right),$$

https://doi.org/10.5194/amt-2021-436
Preprint. Discussion started: 14 January 2022

Atmospheric Measurement Techniques Discussions

$$\Rightarrow D_{fm} > \frac{\log(2\cdot\frac{1+\beta_{AAC}}{1+\beta_{DMA}})}{\log[\frac{2}{1+\beta_{DMA}}\cdot\frac{Cc(d_{m2,min})}{Cc(d_{m1})}]}, \quad (27)$$

This equation describes the minimum value of D_{fm} to eliminate multiple charging effect. It is clearly shown that the mobility resolution of DMA and the relaxation time resolution of AAC determine the limiting condition, and resolution of AAC is more important compared with resolution of DMA. The limiting condition is also related to selected d_m of DMA but independent of selected d_{ae} of AAC (Fig. S1). Setting the same resolutions of DMA and AAC, particle selection is more susceptible to multiple charging effect when selecting small sizes. In Fig. 4a, the values of β_{DMA} and β_{AAC} are 0.1, resulting in the minimum D_{fm} of 1.41, which is the case for most atmospheric aerosol particles. Hence, the selected particles of DMA-AAC are truly monodisperse regardless of particles morphology. However, in actual operations, larger sample flow rate is required to satisfy the apparatus downstream, while the maximum sheath flow rate of classifier is restricted by the instrument design (e.g., 30 L min^{-1} for DMA and 15 L min^{-1} for AAC). When increasing β_{AAC} to 0.3 and remaining β_{DMA} unchanged, the transfer function becomes broader (Fig. 4b). The minimum D_{fm} is 2.44, which indicates that the multiple charging effect exists for typical soot particle with D_{fm} of 2.2-2.4. The line representing soot particles overlaps with the region of doubly charged particles. Thus, reducing resolutions of DMA or AAC is not suggested in actual operations.

3.2 Evaluation of the multiple charging effect

To quantify the possible uncertainties of multiple charging effect in DMA-CPMA system, we conducted the soot experiment as demonstrated in Fig. 1. For each mobility-selected particle, the corresponding d_{ae} and m were determined using scan mode of AAC and CPMA, from which the effective densities were derived, respectively. The results are summarized in table 2. The fitted value of D_{fm} was 2.28, indicating a fractal structure, which is the same as the previous studies (Pei et al., 2018). The effective densities of generated soot particles vary from > 500 kg m^{-3} at d_m = 80 nm to <300 kg m^{-3} at d_m of 250 nm for two methods. In general, the deviation monotonically decreases along with increasing particle size. The deviation is 7.65% for particles of 80 nm, whereas it decreased to <1% of particles lager than 200 nm. The results reveal a strict agreement between two methods for retrieving particle effective density.

According to Fig. 3, the critical slopes of PP_0 for soot particles with d_m of 80, 100, 150, 200 and 250 nm are 2.46, 2.40, 2.29, 2.17 and 2.07, respectively. The measured D_{fm} of 2.28 is smaller than the calculated PP_0 for particles with d_m smaller than 150 nm, which suggested that multiply charged particles are still classified in this circumstance.

When selecting particles with d_m of 80 nm and m of 0.16 fg, the corresponding transfer function is shown in Fig. 5a. The particle population overlaps the transfer function region of doubly charged particles, suggesting the potential interferences of doubly charged particles in DMA-CPMA selection. Since the classification of AAC is insusceptible to particle charging states, the multiply charged particles can be resolved in aerodynamic size distribution. Fig. 5b shows the particles number aerodynamic size distribution ($PNSD_{ae}$) scanned by AAC. $PNSD_{ae}$ was fitted using log-normal distributions and three peaks which correspond to

https://doi.org/10.5194/amt-2021-436
Preprint. Discussion started: 14 January 2022

Atmospheric Measurement Techniques Discussions

singly, doubly and triply charged particles were identified. The mean d_{ae} were 53.8, 58.2 and 69.1 nm, and the corresponding d_{ae} were calculated as 51.1, 61.2 and 69.4 nm using Eq. (1) and Eq. (30), respectively. The experimental results are consistent with the theoretical results with deviation within 5.3%.

On the contrary, when selecting particles with d_m of 200 nm and m of 1.28 fg, the transfer function is shown in Fig. 6a. The slope of PP_0 of 2.07 is smaller than D_{fm} of 2.28, the generated particles population does not overlap with the block of doubly charged particles, thus DMA-CPMA classified particles were truly mono-dispersed. $PNSD_{ae}$ measured by AAC is unimodal, implying that the classified particles were singly charged. The results of other experiments are shown in Fig. S2. Although the transfer function of DMA-CPMA showed that no multiply charged particles would be selected when classifying 150 nm particles (Fig. S2a), doubly charged particles were resolved by AAC (Fig. S2b). These doubly charged particles were selected probably owing to particles diffusion. The non-diffusion models were used to calculate the transfer function but actually the transfer function can be broader because of diffusion. In summary, for a type of particles (with the same mass-mobility relationship), the possibility of multiple charging increases for small particles when selected by DMA-CPMA system, which is consistent with the theoretical calculation in Sect. 3.1.

3.3 Atmospheric implication

The DMA-APM and DMA-CPMA system are usually adopted to eliminate multiply charged particles in soot aerosol studies. As previously discussed, although they might fail to select monodispersed particles, downstream measurements by instrument such as single particle soot photometer (SP2), will not be interfered which characterize the distinct information of single particle. Nevertheless, for techniques measuring properties of entire aerosol population, e.g., scattering coefficient by nephelometer or absorption coefficient by photoacoustic spectrometer， multiply charged particles can induce significant bias. Pervious study (Radney and Zangmeister, 2016) pointed out that DMA-APM failed to resolve multiply charged particles for soot particles when selecting 150 nm flame-generated, which caused 110% error in extinction measurement. In order to investigate the multiple charging effect for DMA-CPMA classification, the optical absorption coefficient of particles with different charging states after DMA-CPMA classification was calculated from $PNSD_{ae}$. Mie theory was used to calculate the theoretical absorption coefficient at the wavelength of 550 nm. The refractive index used in the Mie code was 1.95+0.79i (Bond and Bergstrom, 2006). The $PNSD_{ae}$ for different charging state particles were converted to volume equivalent diameter size distributions ($PNSD_{ve}$) which were used in Mie theory to determine the absorption coefficient for particles with single, double and triple charging, respectively. The method to calculate $PNSD_{ve}$ is described in S1. Then absorption cross-section was derived using the absorption coefficient and integral concentration for particles with different charging states, which denoted as σ_{abs}. For soot particles with diameter of 80 nm, the contributions of particles with different charging states are shown in Fig. 5c. Doubly charged particles only account for 29.6% of the total number concentration but provide the largest fractional contribution in the total absorption (53.1%). Also, small fraction (0.7%) of triply charged particles account for 1.9% of the absorption. As a result, the

https://doi.org/10.5194/amt-2021-436
Preprint. Discussion started: 14 January 2022

mass absorption cross-section (MAC) was overestimated by 54.8% and the directive radiative force (DRF) was overestimated by 54.8%. DRF was calculated using previous global climate models (Bond et al., 2016). Huge amount of 70-90 nm soot particles was emitted from diesel engine (Wierzbicka et al., 2014), neglecting of the multiple charging effect on this size range will result in significant bias in estimation of radiative forcing of automobile emitted soot particles, which may lead to huge error in climate model.

For soot particles with diameter < 200 nm, the optical absorption contributions of particles with different charging state and the MAC overestimation are summarized in Table 3. The number fraction of doubly charged particles declines with the size of nominated particles, i.e. 53.1% and 34.8% for 80 and 100 nm particle, respectively, but only 9.2% for 150 nm particles. Accordingly, the MAC was largely overestimated for 80 and 100 nm particles (54.8% and 27.1%, respectively) but moderately overestimated for 150 nm particles (0.69%). To summarize, our results indicated that the combination of tandem classifiers is not sufficient to completely eliminate multiply charged particles when selecting small size flame-generated soot particle, which introduced severe bias for absorption measurement and leaded to overestimation of MAC, as a result, the DRF of soot particles was also overestimated.

4 Conclusion

In this study, we demonstrate the transfer functions of DMA-CPMA and DMA-AAC and discuss their limitations to eliminate multiply charged particles. For aspherical particles, there is no guarantee that multiple-charging effect can be avoided in DMA-CPMA or DMA-AAC systems. Usually, DMA-AAC can select truly monodisperse particles but it can be suffered of particles with multiple charges when decreasing the resolutions of DMA and AAC. The ability of DMA-CPMA to eliminate multiple charging effect mainly depends on the particles morphology and the instrument resolutions. Under the same setups of DMA-CPMA, this tandem system is more sensitive to multiple charging effect with decreasing D_{fm} and decreasing nominated size of particles. DMA-CPMA failed to eliminate multiply charged particles when selecting soot particles with diameter < 150 nm. Although doubly charged particles accounted for a small fraction of number concentration, they contributed most significantly to light absorption, which indicated that multiply charged particles can induce obvious contribution on light absorption and lead to overestimation of DRF for flame-generated soot particles.

Code/Data availability. Code/Data is available upon request.

Author contributions. ZW determined the main goal of this study. YS and XP designed the methods. YS carried them out and prepared the paper with contributions from all coauthors. YS, HL and JZ analyzed the optical data.

Competing interests. The authors declare that they have no conflict of interest.

Acknowledgements. We specially acknowledge useful comments and suggestions on MATLAB script of CPMA transfer function from Timothy A. Sipkens. The study was supported by the National Natural Science Foundation of China (grant No. 91844301 and 41805100).

https://doi.org/10.5194/amt-2021-436
Preprint. Discussion started: 14 January 2022

Atmospheric Measurement Techniques Discussions

Appendix A

Table A1. Symbol used in this study

μ	Air viscosity
β	The ratio of flow rates of aerosol flow and sheath flow, Q_a/Q_{sh}
τ	Relaxation time
ω_1	Rotational speed of the inner electrode
ω_2	Rotational speed of the outer electrode
$\hat{\omega}$	$\omega_1/\ \omega_2$
δ	Half width of the gap between the two electrodes
Ω	Transfer function
ρ_0	Standard density, which equals to $1 kg/m^3$
τ	Relaxation time
τ^*	τ at the maximum of the transfer function
$\tilde{\tau}$	Dimensionless particle relaxation time, $\tilde{\tau} = \tau/\tau^*$
ρ_{eff}	Effective density
ρ_f	Mass-mobility pre-exponential factor
σ_{cal}	Absorption cross-section calculated with Mie theory
$\sigma_{CAPS-ALB}$	Absorption cross-section measured by CAPS-ALB
B	Mechanical mobility
$C_c(d_p)$	Cunningham slip correction factor
c_r	Particle migration velocity
D_{fm}	Mass-mobility exponent
d_{ae}	Aerodynamic equivalent diameter
d_m	Mobility equivalent diameter
d_{ve}	Volume-equivalence size
e	Elementary charge
L	Length of DMA, CPMA or AAC
m	Particle mass
n	Number of elementary charges on the particle
PNSD	Particle number size distribution
$PNSD_{ae}$	Particle number aerodynamic size distribution
$PNSD_{ve}$	Particle number volume-equivalence size distribution
Q_a	Sample flow rate
Q_{sh}	Sheath flow rate
q	Electrical charge on the particle
R_m	Mass resolution of CPMA

https://doi.org/10.5194/amt-2021-436
Preprint. Discussion started: 14 January 2022

r_a	Lower initial radial position that passes through the classifier
r_b	Upper initial radial position that passes through the classifier
r_1	Inner radius
r_2	Outer radius
$\hat{r}$	r_1/ r_2
t	Time
V	Voltage between the two electrodes of DMA or CPMA
$\bar{v}$	Average flow velocity
v_z	Axial flow distribution
v_θ	Velocity profile in the angular direction
Z_p*	Z_p at the maximum transfer function of DMA
Z_p	Electrical mobility
$\widetilde{Z_p}$	$Z_p/Z_p{}^*$

References

Ait Ali Yahia, L., Gehin, E., and Sagot, B.: Application of the The Rmophoretic Annular Precipitator (TRAP) for the study of soot aggregates morphological influence on their thermophoretic behaviour, J. Aerosol Sci., 113, 40-51, https://doi.org/10.1016/j.jaerosci.2017.07.018, 2017.

Biskos, G., Malinowski, A., Russell, L. M., Buseck, P. R., and Martin, S. T.: Nanosize Effect on the Deliquescence and the Efflorescence of Sodium Chloride Particles, Aerosol Sci. Technol., 40, 97-106, https://doi.org/10.1080/02786820500484396, 2006.

Bond, T. C., and Bergstrom, R. W.: Light Absorption by Carbonaceous Particles: An Investigative Review, Aerosol Sci. Technol, 40, 27-67, https://doi.org/10.1080/02786820500421521, 2006.

Bond, T. C., Doherty, S. J., Fahey, D. W., Forster, P. M., Berntsen, T., DeAngelo, B. J., Flanner, M. G., Ghan, S., Kärcher, B., Koch, D., Kinne, S., Kondo, Y., Quinn, P. K., Sarofim, M. C., Schultz, M. G., Schulz, M., Venkataraman, C., Zhang, H., Zhang, S., Bellouin, N., Guttikunda, S. K., Hopke, P. K., Jacobson, M. Z., Kaiser, J. W., Klimont, Z., Lohmann, U., Schwarz, J. P., Shindell, D., Storelvmo, T., Warren, S. G., and Zender, C. S.: Bounding the role of black carbon in the climate system: A scientific assessment, J. Geophys. Res.: Atmos.: Atmospheres, 118, 5380-5552, https://doi.org/10.1002/jgrd.50171, 2013.

Cheng, Y., Su, H., Koop, T., Mikhailov, E., and Pöschl, U.: Size dependence of phase transitions in aerosol nanoparticles, Nat. Commun., 6, https://doi.org/10.1038/ncomms6923, 2015.

Dastanpour, R., Momenimovahed, A., Thomson, K., Olfert, J., and Rogak, S.: Variation of the optical properties of soot as a function of particle mass, Carbon, 124, 201-211, https://doi.org/10.1016/j.carbon.2017.07.005, 2017.

https://doi.org/10.5194/amt-2021-436
Preprint. Discussion started: 14 January 2022

Dusek, U., Frank, G. P., Hildebrandt, L., Curtius, J., Schneider, J., Walter, S., Chand, D., Drewnick, F., Hings, S., Jung, D., Borrmann, S., and Andreae, M. O.: Size Matters More Than Chemistry for Cloud-Nucleating Ability of Aerosol Particles, Science, 312, 1375-1378, https://doi.org/10.1126/science.1125261, 2006.

Ehara, K., Hagwood, C., and Coakley, K. J.: Novel method to classify aerosol particles according to their mass-to-charge ratio—Aerosol particle mass analyser, J. Aerosol Sci, 27, 217-234, https://doi.org/10.1016/0021-8502(95)00562-5, 1996.

Johnson, T. J., Nishida, R., Irwin, M., Symonds, J. P.R., Olfert, J. S., Boies, A.: Agreement Between Different Aerosol Classifiers Using Spherical Particles, https://doi.org/10.13140/RG.2.2.30999.27043, 2018.

Johnson, T. J.; Nishida, R. T.; Zhang, X.; Symonds, J. P. R.; Olfert, J. S.; Boies, A. M., Generating an aerosol of homogeneous, non-spherical particles and measuring their bipolar charge distribution. J. Aerosol Sci, 153. https://doi.org/10.1016/j.jaerosci.2020.105705, 2021.

Johnson, T. J.; Olfert, J. S.; Cabot, R.; Treacy, C.; Yurteri, C. U.; Dickens, C.; McAughey, J.; Symonds, J. P. R., Steady-state measurement of the effective particle density of cigarette smoke. J. Aerosol Sci, 75, 9-16, https://doi.org/10.1016/j.jaerosci.2014.04.006, 2014.

Kazemimanesh, M., Dastanpour, R., Baldelli, A., Moallemi, A., Thomson, K. A., Jefferson, M. A., Johnson, M. R., Rogak, S. N., and Olfert, J. S.: Size, effective density, morphology, and nano-structure of soot particles generated from buoyant turbulent diffusion flames, J. Aerosol Sci., 132, 22-31, https://doi.org/10.1016/j.jaerosci.2019.03.005, 2019.

Knutson, E. O., and Whitby, K. T.: Aerosol classification by electric mobility: apparatus, theory, and applications, J. Aerosol Sci., 6, 443-451, https://doi.org/10.1016/0021-8502(75)90060-9, 1975.

Kuwata, M.: Particle Classification by the Tandem Differential Mobility Analyzer–Particle Mass Analyzer System, Aerosol Sci. Technol., 49, 508-520, https://doi.org/10.1080/02786826.2015.1045058, 2015.

Moallemi, A.; Kazemimanesh, M.; Corbin, J. C.; Thomson, K.; Smallwood, G.; Olfert, J. S.; Lobo, P., Characterization of black carbon particles generated by a propane-fueled miniature inverted soot generator. J. Aerosol Sci., 135, 46-57, https://doi.org/10.1016/j.jaerosci.2019.05.004, 2019

Olfert, J. S., and Collings, N.: New method for particle mass classification—the Couette centrifugal particle mass analyzer, J. Aerosol Sci., 36, 1338-1352, https://doi.org/10.1016/j.jaerosci.2005.03.006, 2005.

Park, K., Cao, F., And, D. B. K., and Mcmurry, P. H.: Relationship between Particle Mass and Mobility for Diesel Exhaust Particles, Environ. Sci. & Technol., 37, 577-583, https://doi.org/10.1021/es025960v, 2003.

Pei, X., Hallquist, M., Eriksson, A. C., Pagels, J., Donahue, N. M., Mentel, T., Svenningsson, B., Brune, W., and Pathak, R. K.: Morphological transformation of soot: investigation of microphysical processes during the condensation of sulfuric acid and limonene ozonolysis product vapors, Atmos. Chem. Phys., 18, 9845-9860, https://doi.org/10.5194/acp-18-9845-2018, 2018.

Radney, J. G., Ma, X., Gillis, K. A., Zachariah, M. R., Hodges, J. T., and Zangmeister, C. D.: Direct Measurements of Mass-Specific Optical Cross Sections of Single-Component Aerosol Mixtures, Anal. Chem., 85, 8319-8325, https://doi.org/10.1021/ac401645y, 2013.

https://doi.org/10.5194/amt-2021-436
Preprint. Discussion started: 14 January 2022

Radney, J. G., and Zangmeister, C. D.: Practical limitations of aerosol separation by a tandem differential mobility analyzer–aerosol particle mass analyzer, Aerosol Sci. Technol., 50, 160-172, https://doi.org/10.1080/02786826.2015.1136733, 2016.

Rissler, J., Messing, M. E., Malik, A. I., Nilsson, P. T., Nordin, E. Z., Bohgard, M., Sanati, M., and Pagels, J. H.: Effective Density Characterization of Soot Agglomerates from Various Sources and Comparison to Aggregation Theory, Aerosol Sci. Technol., 47, 792-805, 10.1080/02786826.2013.791381, 2013.

Shiraiwa, M., Kondo, Y., Iwamoto, T., and Kita, K.: Amplification of Light Absorption of Black Carbon by Organic Coating, Aerosol Sci. & Technol., 44, 46-54, https://doi.org/10.1080/02786820903357686, 2010.

Sipkens, T. A., Olfert, J. S., and Rogak, S. N.: New approaches to calculate the transfer function of particle mass analyzers, Aerosol Sci. Technol., 54, 111-127, https://doi.org/10.1080/02786826.2019.1680794, 2019.

Stolzenburg, M. R., and McMurry, P. H.: Equations Governing Single and Tandem DMA Configurations and a New Lognormal Approximation to the Transfer Function, Aerosol Sci. Technol., 42, 421-432, https://doi.org/10.1080/02786820802157823, 2008.

Tavakoli, F., and Olfert, J. S.: An Instrument for the Classification of Aerosols by Particle Relaxation Time: Theoretical Models of the Aerodynamic Aerosol Classifier, Aerosol Sci. Technol., 47, 916-926, https://doi.org/10.1080/02786826.2013.802761, 2013.

Tavakoli, F., and Olfert, J. S.: Determination of particle mass, effective density, mass–mobility exponent, and dynamic shape factor using an aerodynamic aerosol classifier and a differential mobility analyzer in tandem, J. Aerosol Sci., 75, 35-42, https://doi.org/10.1016/j.jaerosci.2014.04.010, 2014.

Zangmeister, C. D., You, R., Lunny, E. M., Jacobson, A. E., Okumura, M., Zachariah, M. R., and Radney, J. G.: Measured in-situ mass absorption spectra for nine forms of highly-absorbing carbonaceous aerosol, Carbon, 136, 85-93, https://doi.org/10.1016/j.carbon.2018.04.057, 2018.

Zhang, R., Khalizov, A. F., Pagels, J., Zhang, D., Xue, H., and McMurry, P. H.: Variability in morphology, hygroscopicity, and optical properties of soot aerosols during atmospheric processing, Proc. Natl. Acad. Sci., 105, 10291, https://doi.org/10.1073/pnas.0804860105, 2008.

426 **Table 1 Dimensions of the three classifiers used for transfer function calculation**

Parameter	DMA	CPMA	AAC
r_1 (mm)	9.37	100	43
r_2 (mm)	19.61	103	45
L (mm)	44.369	200	210
ω_2/ω_1	—	0.945	—

427

428 **Table 2. Mobility diameter, mass, aerodynamic diameter, effective densities calculated by DMA-AAC and DMA-**
429 **CPMA, and the deviation between them for fresh soot particles in the size range of 80-250 nm.**

d_m(nm)	m(fg)	d_{ae}(nm)	$\rho_{DMA\text{-}AAC}$ (kg m^{-3})	$\rho_{DMA\text{-}CPMA}$ (kg m^{-3})	Deviation
80	0.16	48	551.2	596.8	7.65%
100	0.27	55	488.0	515.7	5.38%
150	0.66	67	359. 1	373.5	3.86%
200	1.28	82	303.2	305.6	0.77%
250	2.17	96	262.8	265.2	0.90%

430

431 **Table 3. Number concentration fractions and absorption contributions for different size fresh soot particles with**
432 **single, double or triple charges and the overestimation of MAC accordingly.**

d_m (nm)	**singly charged particles**		**doubly charged particles**		**triply charged particles**		**MAC overestimation**
	f_N	**f_{abs}**	**f_N**	**f_{abs}**	**f_N**	**f_{abs}**	
80	69.7%	45.0%	29.6%	53.1%	0.7%	1.9%	54.8 %
100	82.9%	65.2%	17.1%	34.8%	-	-	27.1 %
150	97.0%	90.8%	3.0%	9.2%	-	-	0.69 %

433

https://doi.org/10.5194/amt-2021-436
Preprint. Discussion started: 14 January 2022

Atmospheric Measurement Techniques
Discussions

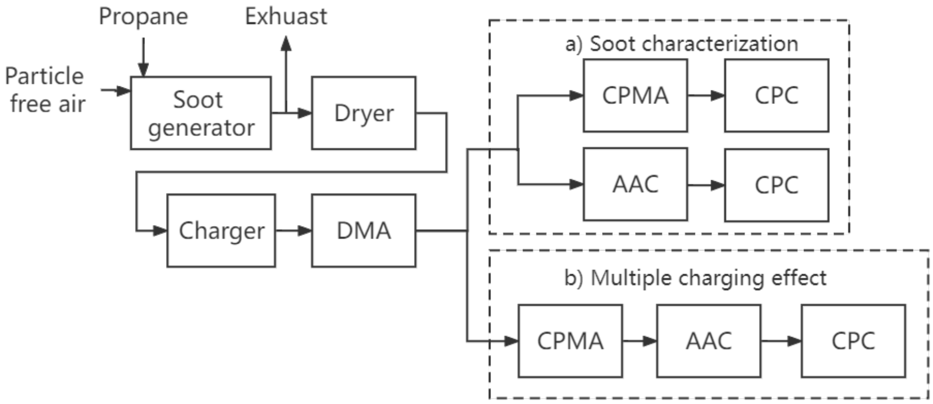

Figure 1: Schematic of the experimental setup: (a) soot characterization and (b) evaluation of multiple charging effects.

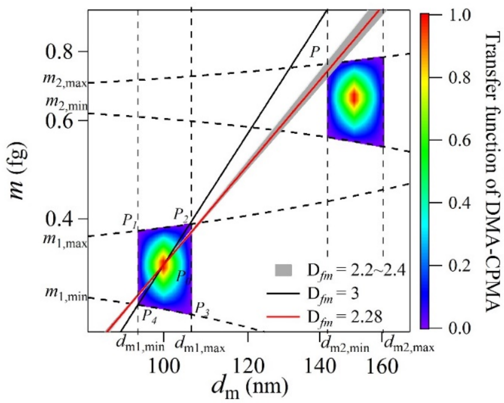

Figure 2: Example of DMA-CPMA transfer function. The following parameter set was employed for the calculations: dm = 100 nm, βDMA = 0.1, m = 0.33 fg, QCPMA=0.3 L min-1, Rm = 8. The color blocks are the transfer function of DMA-CPMA with the rainbow color representing the transfer function for singly charged (lower left block) and doubly charged (upper right block) particles. The black and red solid lines are particles population with Dfm of 3 and 2.28, respectively. The grey region is particle population with Dfm of 2.2-2.4, which is typical for soot aerosols. The dashed lines are the limits of dm and m of DMA and CPMA. The DMA–CPMA transfer function for +2 particles does not overlap with the line for spherical particles with single charge (Dfm=3).

https://doi.org/10.5194/amt-2021-436
Preprint. Discussion started: 14 January 2022

Atmospheric Measurement Techniques
Discussions

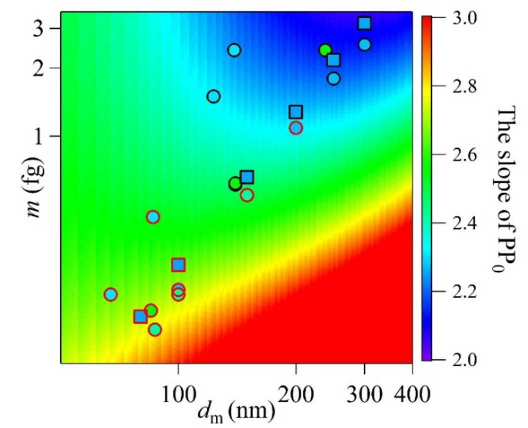

Figure 3: Variations of the slope of PP_0 as a function of classified d_m and m. The following parameter set was employed for the calculations: β_{DMA} = 0.1, Q_{CPMA}=0.3 L min^{-1}, R_m = 8. The background color coding denotes the slope of PP_0 with red represents the slope of $PP_0 \geqslant 3$. The circles and squares represent the reported D_{fm} values from literatures (Park et al., 2003; Rissler et al., 2013; Ait Ali Yahia et al., 2017; Dastanpour et al., 2017; Kazemimanesh et al., 2019) and measured soot particles in this study (See details in section 3.2), respectively. Symbol colors indicate the particle D_{fm}. Symbols with red border correspond to the cases that potential multiple charging effect may exist.

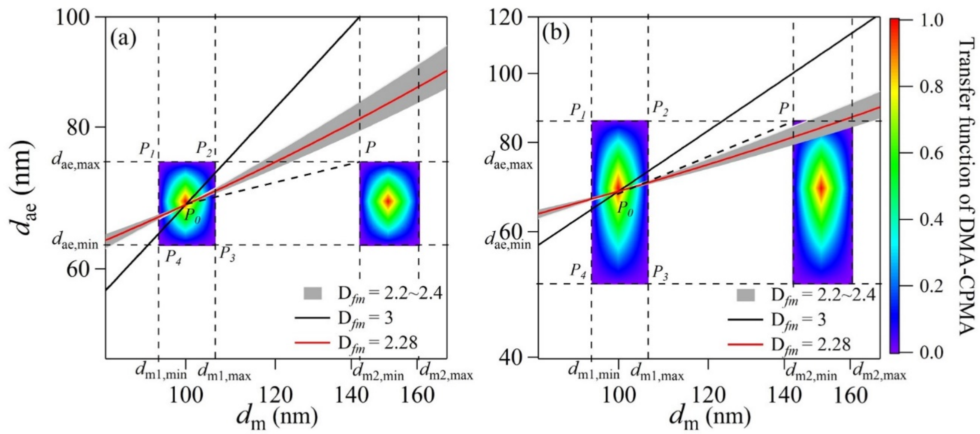

Figure 4: Example of transfer function calculation of DMA-AAC. The following parameter set was employed for the calculations: Q_a=0.3 L min^{-1}, d_{m1} = 100 nm, d_{ae} = 68.3 nm, (a) β_{DMA} = 0.1, β_{AAC} = 0.1, (b) β_{DMA} = 0.1, β_{AAC} = 0.3. The color blocks are the transfer functions of DMA-AAC. The black and red solid lines are particles population with D_{fm} of 3 and 2.28, respectively. The grey region is particle population with D_{fm} of 2.2-2.4, which is typical for soot aerosols. The black dashed lines are the limiting d_m and d_{ae} of DMA and AAC.

https://doi.org/10.5194/amt-2021-436
Preprint. Discussion started: 14 January 2022

Atmospheric Measurement Techniques
Discussions

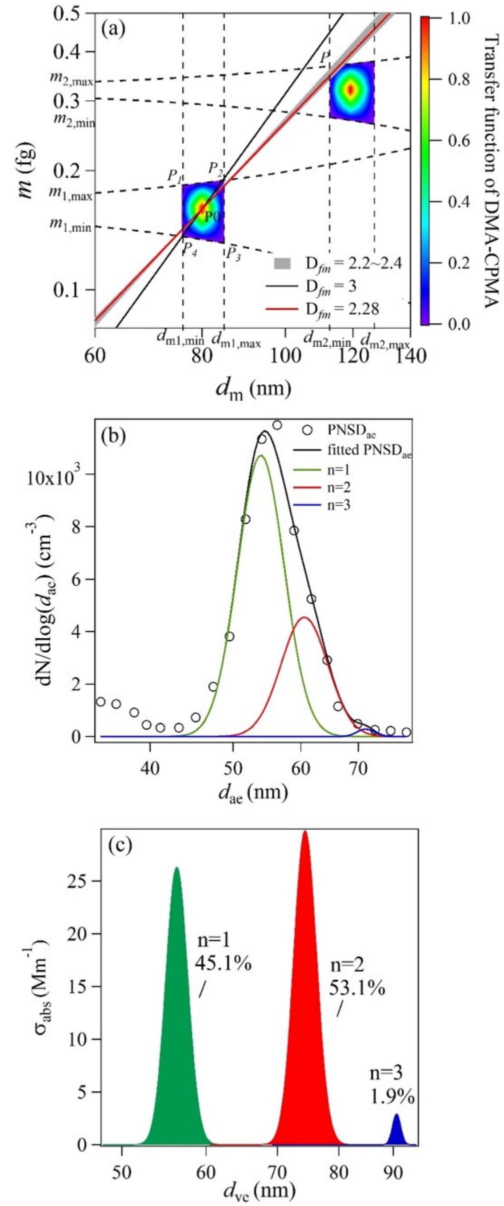

Figure 5: (a) The transfer functions of DMA-CPMA when selecting 80 nm particles. The following parameter set was employed for the calculations: d_{m1} = 80 nm, β_{DMA} = 0.1, m_1 = 0.16 fg, Q_{CPMA}=0.3 L min^{-1}, R_m = 8. The red solid line is the generated soot particle population. (b)The aerodynamic size distribution of particles classified by DMA-CPMA. The circles are data measured by AAC-CPC and the black, green red and blue lines are log-normal fitted distributions of bulk, singly charged, doubly charged and triply charged particle population. (c)The contributions to light absorption of particles with single, double and triple charges calculated with Mie theory.

https://doi.org/10.5194/amt-2021-436
Preprint. Discussion started: 14 January 2022

Atmospheric Measurement Techniques Discussions

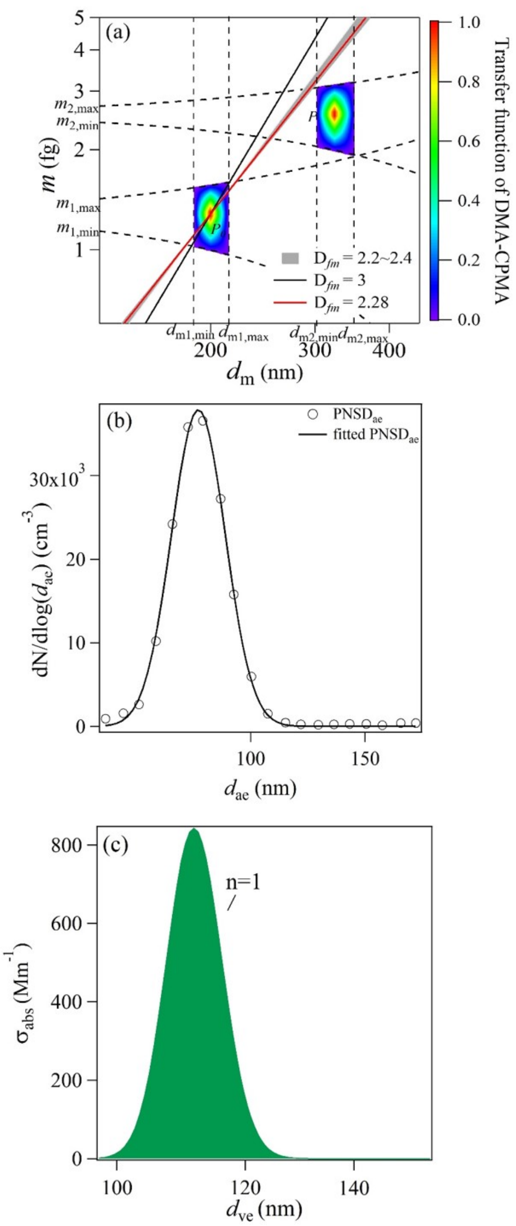

Figure 6: (a)The transfer functions of DMA-CPMA when selecting 200 nm particles. The following parameter set was employed for the calculations: d_{m1} = 200 nm, β_{DMA} = 0.1, m_1 = 1.28 fg, Q_{CPMA}=0.3 L min^{-1}, R_m = 8. The red solid line is the generated soot particle population. (b)the aerodynamic size distribution of particles classified by DMA-CPMA. The circles are data measured by AAC-CPC and the solid line is log-normal fitted distribution. (c)the contributions to light absorption of particles with single charge calculated with Mie theory.